Band offsets and density of Ti^{3+} states probed by x-ray photoemission on $LaAlO_3/SrTiO_3$ heterointerfaces and their $LaAlO_3$ and $SrTiO_3$ bulk precursors

G. Drera,[1] G. Salvinelli,[1] A. Brinkman,[2] M. Huijben,[2] G. Koster,[2] H. Hilgenkamp,[2] G. Rijnders,[2] D. Visentin,[1] and L. Sangaletti[1]

[1]*Interdisciplinary Laboratories for Advanced Materials Physics and Dipartimento di Matematica e Fisica, Università Cattolica, via dei Musei 41, 25121 Brescia, Italy*

[2]*MESA + Institute for Nanotechnology, University of Twente, P.O. Box 217, 7500 AE Enschede, Netherlands*

(Received 7 August 2012; published 25 February 2013)

A set of $LaAlO_3/SrTiO_3$ (LAO-STO) interfaces has been probed by x-ray photoemission spectroscopy in order to contrast and compare the effects of LAO overlayer thickness and of the growth conditions on the electronic properties of these heterostructures. These effects are tracked by considering the band offset and the density of Ti^{+3} states, respectively. It is shown that the dominant effects on the local electronic properties are determined by the O_2 partial pressure during the growth. In particular, a low P_{O_2} yields Ti^{+3} states with higher density and lower binding energy compared to the sample grown at high P_{O_2} or to the bare STO reference sample. Band-offset effects are all below about 0.7 eV, but a careful analysis of Ti $2p$ and Sr $3d$ peaks shows that valence-band offsets can be at the origin of the observed peak width. In particular, the largest offset is shown by the conducting sample, which displays the largest Ti $2p$ and Sr $3d$ peak widths.

DOI: 10.1103/PhysRevB.87.075435 PACS number(s): 73.20.−r, 79.60.Jv, 74.78.Fk, 73.40.−c

I. INTRODUCTION

Lanthanum aluminate ($LaAlO_3$, LAO for short) and strontium titanate ($SrTiO_3$, STO) are formally band insulators, as they are closed-shell compounds ($4f^0$ for LAO and $3d^0$ for STO), with a band gap of 5.4 and 3.2 eV, respectively. These materials belong to the perovskite group, sharing the same chemical formula (ABO_3) and a similar cubic crystal structure. When a LAO-STO heterointerface is created, a p-type heterostructure is expected if the bulk STO is terminated with a SrO plane (hole doping), while an n-type heterostructure should be obtained with a TiO_2 plane (electron doping) termination. In the latter case, the LAO-STO interface becomes conducting[1] and yields a quasi-two-dimensional electron gas (quasi-2DEG). The transition to the metallic state was found to be thickness dependent: the 2DEG is observed only when the LAO capping is at least 4 unit cells (u.c.) thick.[2] The main difference between LAO and STO resides in the layer charge polarity:[3] looking at the (001) planes, STO is a nonpolar solid since both $Sr^{2+}O^{2-}$ and $Ti^{4+}O_2^{2-}$ planes are charge neutral, while LAO is a polar solid, as it is composed of $La^{3+}O^{2-}$ and $Al^{3+}O_2^{2-}$ charged layers. The p-type interface is thus formed by $SrO\text{-}(AlO_2)^{1-}$ planes, while the n-type is formed by $TiO_2\text{-}(LaO)^{1+}$ planes. The observed conductivity was originally thought to be the response of the system to the diverging potential (the so-called polar catastrophe[4,5]) created by LAO.

In nonoxide semiconductors, the relaxation of polar discontinuity in heterointerfaces is usually achieved by an atomic reconstruction process,[1] where the interface stoichiometry is altered by interdiffusion, point defect, and dislocation and in general by a structural roughening. In oxides, the possibility of multiple valence ions allows also an electronic reconstruction that, in the LAO-STO case, should move electrons from the surface to the empty Ti d levels, leading to $3d^1$ electronic states. A 2D lattice of electrons in a correlated material can originate phenomena like a metal-insulator transition (MIT), localized magnetic moments, and even superconductivity;[6,7] most of these effects have been observed in LAO-STO, although not all in one sample at the same time.

In principle, both atomic and electronic reconstructions could be present in the LAO-STO case. For example, there is much experimental proof of interdiffusion[8,9] (with La ions drifting inside STO, a form of atomic reconstruction), but this mechanism alone cannot be solely responsible of the conductivity.

Electronic reconstruction, an electronic rearrangement aimed at avoiding polar catastrophe, may also occur in both p-type and n-type interfaces. An extra electron is expected in n-type interfaces to fill Ti empty states, while an extra hole is required for p-type interfaces. However, this charge rearrangement does produce an asymmetric behavior in the two junctions. While metallic conductivity and Hall measurements suggest the presence of a delocalized electron at the n-type interface, the p-type interface is found to be insulating. In the former case, extra electrons are placed in the otherwise empty Ti states, while for p-type interfaces there are no energetically favorable electronic states to host the extra hole, and the compensation occurs through the creation of oxygen vacancies at the interface, yielding to an atomic interface reconstruction.[4] This asymmetry was more recently related to a different extent of the polarization region and atomic intermixing at the LAO-STO interface, which ultimately led to distinct band-bending effects and to the contrast in electrical conductivity between n-type and p-type interfaces.[10]

The n-type interface is known to become conducting for a LAO thickness above 4 u.c. The thickness dependence of conductivity could be explained by a band-bending effect,[11] induced by polarity discontinuity: the density of states (DOS) of the LAO valence band (VB) should be shifted to higher binding energies (BE) until, for a capping equal to or greater than 4 u.c., the VB maximum is superimposed to the buried empty levels of STO. The conduction should now be triggered by a tunneling effect from the surface to the interface. However,

a significant band bending has not yet been observed in terms of core-level shift, while a shift of 3.2 eV (needed to span the electronic gap in STO) should be easily observed.

Finally, the sample growth conditions deeply affect the transport properties; an oxygen-poor growth atmosphere can induce oxygen vacancies and thus a 3D conductivity,[12–15] while an excessively rich one can even result in a 3D growth and thus in a different kind of heterostructure.[6] Depending on the O_2 partial pressure during growth, three phases are usually identified:[7,16] one dominated by oxygen vacancies contribution ($P_{O_2} \simeq 10^{-6}$ mbar), one displaying superconductivity ($P_{O_2} \simeq 10^{-5}$mbar), and one displaying a magnetic behavior ($P_{O_2} \simeq 10^{-3}$ mbar). It is quite a challenging task to find a unified description of all these phenomena.

The experimental signatures of many of the proposed models are the LAO-STO band offset and the density and distribution of Ti^{3+} states. Recently, these states have been evidenced by soft x-ray photoemission with photon energy tuned at the Ti $2p$-$3d$ threshold.[17,18] Also core-level x-ray photoelectron spectroscopy (XPS) can provide an indication of Ti^{3+} states, as reported in Refs. 18 and 19 and in hard x-ray photoelectron spectroscopy (HAXPES) experiments.[20] At odds with Refs. 17–19, Ref. 8 did not report on observed Ti^{3+} features in Ti $2p$ core-level photoemission. As for valence-band offsets (VBO), core-level shifts much smaller than those predicted by the polar catastrophe have been observed by Takizawa *et al.*,[19] Chambers *et al.*,[8] and Segal *et al.*,[21] but it is not yet possible to draw a consistent picture of VBO as the results show, in some cases, opposite trends.

In the present study, a spectroscopic investigation of insulating and conductive LAO-STO films is carried out by XPS. We address the problem of the spectroscopic signature of the interface effects by comparing several LAO-STO interfaces with their LAO and STO bulk precursors. We checked to what extent the electronic properties of LAO-STO can be described as a weighted (i.e., thickness dependent) superposition of those of LAO and STO, as deviations from this mere superposition should be regarded as a signature of new electronic states arising from the heterointerface buildup.

Following this approach, we show that the different LAO overlayer thicknesses affect the electronic properties of the interfaces in terms of band offsets, although smaller than those theoretically predicted, whereas the dominant effects on the local electronic properties are related to the O_2 partial pressure during the growth. This is seen by tracking the Ti^{3+}/Ti^{4+} ratio for Ti $2p$ core levels and the Sr $3d$ and Ti $2p$ core-level line widths. Although band offsets are all below about 0.7 eV, differences are detected among the samples, and it is shown that the Ti $2p$ and Sr $3d$ peak widths scale with band offsets, with the larger values being found for the 5-u.c. conducting sample. Finally, a careful analysis of the Ti^{3+}/Ti^{4+} peak area ratio based on the depth distribution function of photoelectrons allowed us to set a lower limit to the density of Ti^{3+} states across the interface as seen by the present photoemission experiment.

II. EXPERIMENTAL DETAILS

The LAO-STO heterostructures (HS) have been grown by pulsed laser deposition (PLD) at the MESA$^+$ Institute for Nanotechnology, University of Twente. The two n-type 3-u.c. and 5-u.c. LAO-STO samples were grown in a $P_{O_2} \sim 10^{-3}$ mbar oxygen partial pressure. In addition, an *insulating* n-type 5-u.c. LAO-STO sample, grown at 10^{-1} mbar O_2 partial pressure, has been analyzed. The 3-u.c. sample and the insulating 5-u.c. sample showed a sheet resistance above 1 GΩ/□, while the conducting 5-u.c. sample showed a sheet resistance of 5.5 KΩ/□ at 300 K. Two reference single-crystal LAO and STO samples terminated with the (001) surface have also been considered (MaTeck GMBH). The sample list is reported in Table I. XPS has been used to measure the core-level electronic structure and to evaluate the stoichiometry of the heterostructures. The XPS data have been collected at the Surface Science and Spectroscopy Laboratory of the Università Cattolica (Brescia, Italy) with a nonmonochromatized dual-anode PsP x-ray source; the Mg $K\alpha$ line ($h\nu = 1253.6$ eV) has been used to achieve a better resolution (about 0.7 eV), while the Al $K\alpha$ line ($h\nu = 1486.6$ eV) has been used when the maximum probing depth was needed. The analyzer for XPS was a SCIENTA R3000, operating in the transmission mode, which maximizes the transmittance and works with a 30° acceptance angle.

In XPS, the core-level peak area of a selected layer at a depth d with a thickness t can be evaluated through the following formula:

$$I(E_k,\alpha) = K \int_d^{d+t} \Phi(E_k,\alpha,z)dz, \qquad (1)$$

where K is a normalization constant, which includes the photoionization cross section,[22] the atomic density of the species, and analyzer-dependent parameters; $\Phi(E_k,\alpha,z)$ is the generic escape probability (known as the depth distribution function, DDF) of an electron generated at a depth

TABLE I. Ti^{3+}/Ti^{4+} peak area ratio, energy shift Δ(BE) between the Ti^{4+} and Ti^{3+} core-level peaks, full width at half maximum (FWHM) of Ti $2p$ and Sr $3d$ peaks, Ti $2p$ peak broadening σ_{EXTRA} with respect to the STO case, and sheet charge density (SCD) evaluated assuming a Ti^{3+} distribution across a 1-u.c.- or a 2-u.c.-thick layer below the interface.

	P_{O_2} (10^{-3} mbar)	Ti^{3+}/Ti^{4+} XPS ratio	Δ(BE) Ti^{4+}-Ti^{3+} (eV)	Ti $2p$ FWHM (eV)	Sr $3d$ FWHM (eV)	σ_{EXTRA} (Ti $2p$) (eV)	SCD 1 u.c.	SCD 2 u.c.
5 u.c. conducting	1.0	0.056 ± 0.005	2.03	1.47	1.24	0.56	1.50×10^{14}	1.68×10^{14}
3 u.c. insulating	1.0	0.012 ± 0.005	2.10	1.43	1.18	0.44	3.70×10^{13}	4.00×10^{13}
5 u.c. insulating	100	0.006 ± 0.005	1.78	1.41		0.37		
STO		0.004 ± 0.005	1.73	1.36	1.05	0.00		

z with a kinetic energy E_k at an angle α respect to the surface normal. According to the Lambert-Beer law, the DDF function is usually approximated with a Poisson distribution $\Phi = e^{-z/\lambda Cos(\alpha)}$, where λ is the inelastic mean free path (IMFP). Even if it leads to simple analytical expressions for the peak areas, such an approximation (defined as straight line motion by Tilinin *et al.*[23]) is known to be quantitatively wrong and, especially for the present thin overlayers, can result in an overestimated capping thickness.

In this work, we resorted to Monte Carlo (MC) DDF calculations, with the algorithm described in Ref. 24, in order to include inelastic as well as elastic electronic scattering in the so-called transport approximation[25] (TA). The photoemission asymmetry parameters have been taken into account for each core level. Monte Carlo calculations of electron trajectories have been carried out in order to predict the XPS peak areas in LAO-STO heterostructures since an analytic DDF formulation[23] cannot be written for a generic multilayer sample.

III. RESULTS AND DISCUSSION

A. Core level and valence-band photoemission

The La 4*d* and Al 2*s* XPS shallow core levels are shown in Fig. 1(a). All spectra are normalized to the Al 2*s* peak. As can be observed, for the 5-u.c. conducting and the 3-u.c. insulating samples the La 4*d* core levels are superposed, with an intensity below that of the LAO reference crystal. In turn, the La 4*d* XPS core lines of the 5-u.c. insulating sample display the largest intensity. These features are qualitatively consistent with the results reported in literature[26] and suggest that the P_{O_2} value has a relevant effect on the cation stoichiometry in the LAO overlayer. This is not unexpected, as the 5-u.c. insulating sample is known to show a 3D growth regime rather than the layer-by-layer regime for the other two heterostructures grown at lower P_{O_2}. It has been observed[26] that among possible defects related to a La excess with respect to Al, the formation of Al vacancies seems to be the most likely scenario. In turn, the low La intensity of the heterostructures grown at low P_{O_2} compared to the case of the LAO single crystal apparently shows a La deficiency that could be related to La diffusion through the interface, La substoichiometry, or both.

The O 1*s* spectra from the three heterostructures are shown in Fig. 1(b). It is important to note that the three spectra are virtually identical, in spite of the different growth conditions and thicknesses of the LAO overlayer. This assures that in all cases a similar oxygen stoichiometry can be estimated at the surface, ruling out the possibility that changes at the interface could be ascribed to major differences in the oxygen stoichiometry on the surface.

In Fig. 2 the valence-band spectra, collected with the Mg $K\alpha$ x-ray source, are shown. The shallow core levels are labeled as S_I, S_{II}, and S_{III}. The O 2*s* states mostly contribute to the S_I peak, Sr 4*p* is an unresolved doublet below the S_{II} peak, and La 5*p* is split in S_{II} and S_{III} peaks (the spin-orbit energy separation is about 2.4 eV, as detected in, e.g., La_2O_3; Ref. 27). It is possible to describe the LAO-STO spectra as the linear combination of the single-crystal spectra. Starting from the LAO and STO spectra as displayed in Fig. 2, the VBs of

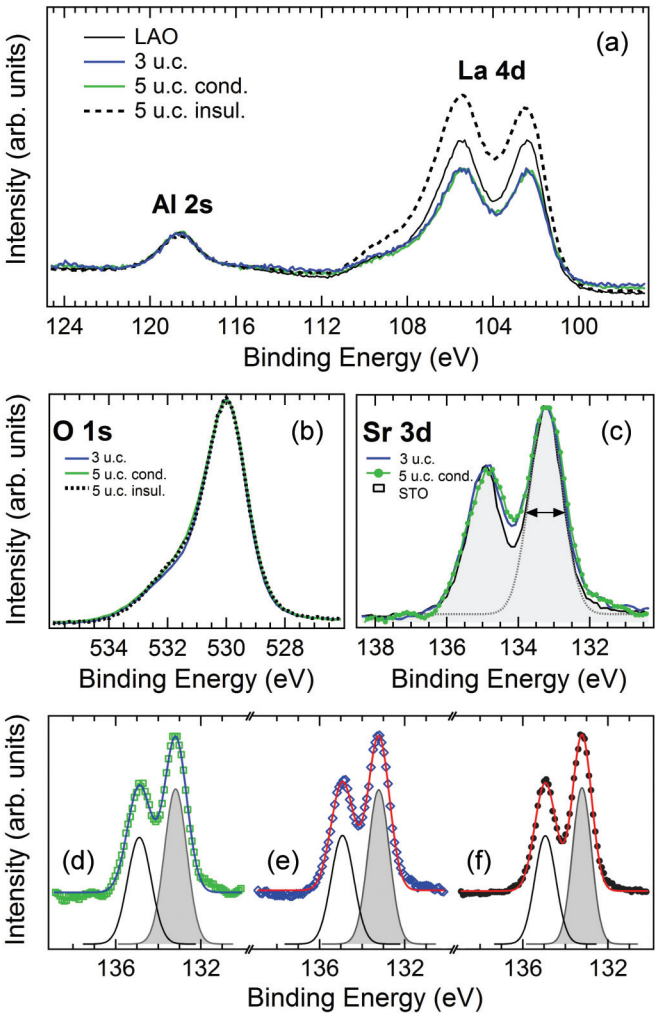

FIG. 1. (Color online) (a) Al 2*s* and La 4*d* XPS spectra collected from LAO and the LAO-STO heterostructures. Spectra have been normalized to the Al 2*s* peak area. (b) O 1*s* XPS spectra of the three HS and (c) Sr 3*d* XPS spectra of the STO single crystal and the two HS grown at low P_{O_2}. The bottom panel shows the Sr 3*d* XPS core-level data fitting of the (d) 5-u.c. conducting, (e) 3-u.c. insulating, and (f) STO samples.

the three LAO-STO samples have been calculated as a linear combination of the bulk precursor spectra where two fitting parameters have been considered, i.e., the energy shift of the LAO VB spectrum with respect to the STO VB spectrum and the relative integrated intensity of these two VB spectra. The results of this procedure are shown in Fig. 2 (thin lines). In all cases, there is a slight difference (below 0.2 eV) among the energy shifts resulting from the best fit of the three LAO-STO interfaces (Table II: LAO vs STO BE shift). If band bending is present, such a small difference is unable to be the sole cause of the buildup of the 2DEG.

On the intensity side, the accuracy of the fitting results can be checked by evaluating if the STO signal attenuation obtained from the fitting is consistent with the thickness of the LAO overlayer. Defining the integrated intensity of the XPS signal referred to STO as I_{STO}, then the STO signal attenuation of the 5-u.c. (thickness $= d_5$) sample with respect to the 3-u.c.

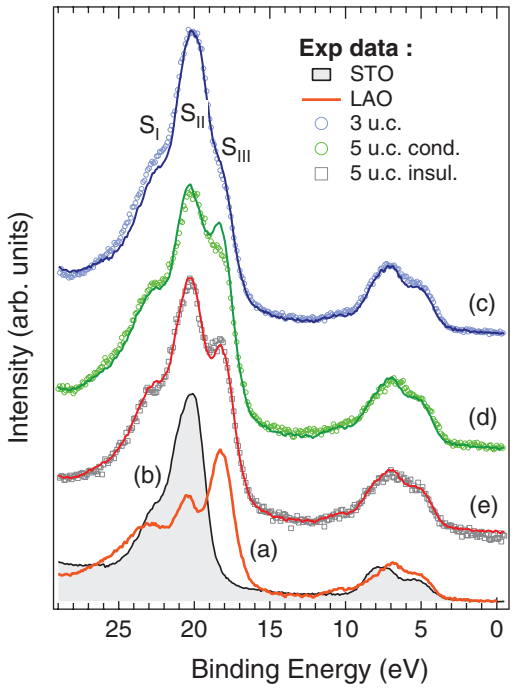

FIG. 2. (Color online) XPS valence band and shallow-core-level spectra of LAO and STO single crystals [lines (a) and (b)] and LAO-STO heterostructures [lines (c)–(e)]. The LAO-STO valence bands [lines (c)–(e)] have been fitted with a linear combination of the LAO and STO spectra shown in lines (a) and (b).

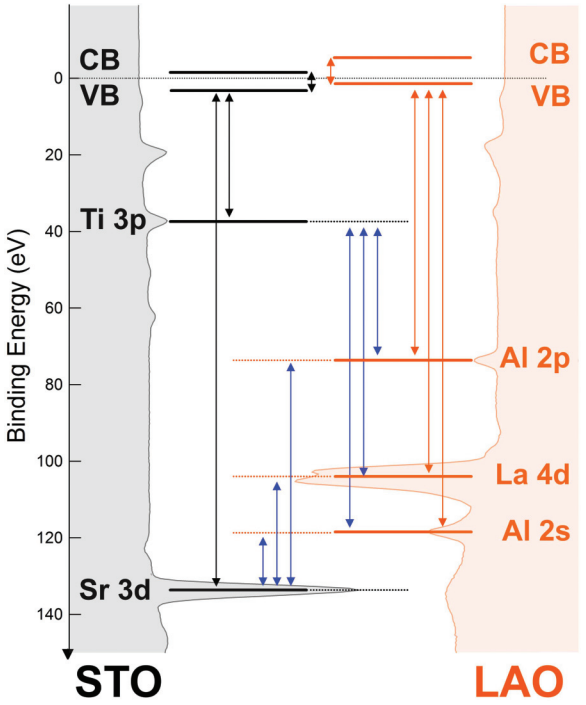

FIG. 3. (Color online) Schematic of energy levels involved in the band-offset calculations. The STO core levels are reported on the left side, while the LAO core levels can be found on the right side. The shaded areas show the XPS data collected from the STO and LAO bulk crystals.

(d_3) sample can be written as

$$\frac{I_{\mathrm{STO5u.c.}}}{I_{\mathrm{STO3u.c.}}} = \frac{\int_{d_5}^{+\infty} \Phi_{\mathrm{LAO_{d5}-STO}}(E_k,\alpha,z)dz}{\int_{d_3}^{+\infty} \Phi_{\mathrm{LAO_{d3}-STO}}(E_k,\alpha,z)dz}, \qquad (2)$$

while this ratio is experimentally determined to be about 0.59 for the two samples grown at low P_{O_2}. Solving the equation to extract the thickness difference between the two layers, a value of $d_5 - d_3 = 9$ Å is obtained, in good agreement with the expected $5 - 3 = 2$ u.c. thickness (7.6–7.8 Å). This makes the signal attenuation evaluated from the VB and shallow core levels consistent, providing also positive feedback on the results about the negligible LAO-STO valence-band offset among the samples. It is also worth noting that measured peak S_{III}, ascribed to La $5p_{3/2}$, in the 5-u.c. conducting sample [Fig. 2(d)] is lower than the calculated peak. This is consistent with the fact the this sample has been evaluated as La poor from the shallow-core-level analysis (Fig. 1). Finally, we observe that the use of the inelastic mean free path alone rather than the DDF would yield a $d_5 - d_3 = 13.3$ Å value, clearly in contrast to the expected thickness. This further shows the inadequacy of the IMFP concept in the estimation of attenuation lengths.

B. Binding-energy shifts and band offsets

Possible band offsets can also be measured by considering the BE difference between a core line from a LAO element and a core line of an STO element. Following Ref. 8, we have evaluated the following differences:

$$\Delta E_V^{La4d-Sr3d} = (E_{La4d} - E_V)_{\mathrm{LAO}} - (E_{Sr3d} - E_V)_{\mathrm{STO}} + (E_{Sr3d} - E_{La4d})_{HJ}, \qquad (3)$$

$$\Delta E_V^{Al2s-Sr3d} = (E_{Al2s} - E_V)_{\mathrm{LAO}} - (E_{Sr3d} - E_V)_{\mathrm{STO}} + (E_{Sr3d} - E_{Al2s})_{HJ}, \qquad (4)$$

$$\Delta E_V^{La4d-Ti3p} = (E_{La4d} - E_V)_{\mathrm{LAO}} - (E_{Ti3p} - E_V)_{\mathrm{STO}} + (E_{Ti3p} - E_{La4d})_{HJ}, \qquad (5)$$

TABLE II. Calculated BE shift between core-level peaks, calculated according to Eqs. (3) to (8), and LAO vs STO VB spectra energy shift obtained by fitting the LAO-STO VB spectra. For each sample, ave. core is average BE shift obtained from the six values extracted through Eqs. (3) to (8). All energies are in eV.

	La $4d_{5/2}$–Sr $3d$	Al $2s$–Sr $3d$	La $4d_{5/2}$–Ti $3p$	Al $2s$–Ti $3p$	Al $2p$–Ti $3p$	Al $2p$–Sr $3d$	ave. core	LAO vs STO VB shift
5 u.c. conducting	−0.46	−0.54	−0.89	−0.97	−0.94	−0.52	−0.72 ± 0.24	−0.04
3 u.c. insulating	−0.56	−0.61	−0.74	−0.79	−0.75	−0.57	−0.67 ± 0.10	−0.10
5 u.c. insulating	−0.34	−0.27	−1.01	−0.94	−0.77	−0.10	−0.57 ± 0.38	+0.17

$$\Delta E_V^{Al2s-Ti3p} = (E_{Al2s} - E_V)_{\mathrm{LAO}} - (E_{Ti3p} - E_V)_{\mathrm{STO}} + (E_{Ti3p} - E_{Al2s})_{HJ}, \quad (6)$$

$$\Delta E_V^{Al2p-Ti3p} = (E_{Al2p} - E_V)_{\mathrm{LAO}} - (E_{Ti3p} - E_V)_{\mathrm{STO}} + (E_{Ti3p} - E_{Al2p})_{HJ}, \quad (7)$$

$$\Delta E_V^{Al2p-Sr3d} = (E_{Al2p} - E_V)_{\mathrm{LAO}} - (E_{Sr3d} - E_V)_{\mathrm{STO}} + (E_{Sr3d} - E_{Al2p})_{HJ}, \quad (8)$$

which can be identified by referring to the diagram of Fig. 3, where the energy levels involved in the calculations for both the reference LAO and STO single crystals and the LAO-STO heterostructure are shown. The results are reported in Table II. As can be observed, when averaged over the six different combinations, all differences are within 0.15 eV (Table II, ave. core), in agreement with the results obtained from the VB data analysis (0.21 eV; Table II: LAO vs. STO VB shift).

Several studies on the band lineup have been published so far, but it is rather difficult to find a rationale among them. One group of studies is focused on core-level differences between *p*-type and *n*-type samples. Takizawa *et al.*[19] have focused on the band lineup of *p*-type and *n*-type interfaces, both with 1, 3, 4, 5, and 6 LAO u.c. overlayers. They show that core levels belonging to the same layer of the HS (i.e., La and Al for LAO and Ti and Sr for STO) do not show appreciable shifts (less than 100 meV). In turn, an energy shift is observed for the Al 2*p*–Sr 3*d* BE difference. This shift increases with the number of LAO u.c. for both *p*- and *n*-type samples. The interfaces have been grown by PLD in a 1×10^{-5} Torr oxygen partial pressure. Segal *et al.*[21] present a similar study, where *p*-type and *n*-type interfaces with 2 to 9 LAO u.c. have been investigated and the Sr 3*d*–La 4*d* BE difference has been tracked. Here, this energy difference is found to change with the number of layers, but while it increases for *p*-type samples, it decreases for *n*-type samples. The samples have been grown by molecular beam epitaxy (MBE) in 3×10^{-7} Torr oxygen partial pressure. Yoshimatsu *et al.*[28] investigate the Ti 2*p* BE shift for both *p*-type and *n*-type samples (0 to 6 LAO u.c., laser MBE, 1×10^{-5} Torr). In this case, the Ti 2*p* BE for the *p*-type samples is found to be constant, while for the *n*-type samples the BE decreases with LAO thickness.

Unlike the papers mentioned so far, Chambers *et al.*[8] did not consider the *p*-type and *n*-type set of samples but focused on two 4-u.c. *n*-type samples grown at rather similar O_2 pressures (1×10^{-5} and 8×10^{-6} Torr). A set of BE differences have been evaluated, namely, Sr 3*d*–La 4*d*, Sr 3*d*–Al 2*p*, Ti 2*p*–La 4*d*, and Ti 2*p*–Al 2*p*. Furthermore these differences were referenced to the VBO, a procedure neglected in the previous studies. The present study follows this pathway, but important differences emerge with respect to Chambers *et al.*'s results. It is rather interesting to note that in the samples considered in Ref. 8 the Ti^{3+} contribution is not detected on the low-BE of the Ti $2p_{3/2}$ XPS peak. In the samples presented here we detect Ti^{3+} states in Ti 2*p* core lines, which find a counterpart in the $3d^1$ electron emission in the valence-band region probed by resonant photoemission (RESPES), as can be found in Ref. 29 (Chap. 5), similar to the data presented in a previous investigation.[17] Furthermore, while Chambers *et al.*[8] detect similar BE energy differences in the same sample, irrespective of the couple of atoms selected, we detect much different changes within the same sample. When Ti is involved as one of the core levels in Eqs. (5)–(7), larger shifts are usually detected with respect to those resulting from Eqs. (3), (4), and (8). This seems to indicate that in our sample it is possible to observe element-specific shifts, while in the samples examined by Chambers *et al.*[8] the shifts are rather uniformly distributed. This is tentatively ascribed to the fact that localized Ti^{3+} states at the interface may have much larger effects on the local electronic properties than the widespread charge distribution invoked by Chambers *et al.* to justify the lack of a Ti^{3+} low-BE feature in Ti 2*p* XPS spectra.

C. Ti 2*p* core levels

In Fig. 4 the Ti 2*p* XPS core lines of the 3-u.c. and the two 5-u.c. heterointerfaces and the pure STO are shown. The Ti 2*p* spectrum is almost identical to that expected for a Ti^{4+} ion. However, a small bump is detectable on the low-BE side of the 5-u.c. spectrum, in the position usually associated with Ti^{3+} electronic states. These states can be detected only through a comparison among different samples and can be easily confused as an additional experimental broadening of the Ti $2p_{3/2}$ peak. For this reason we also show the Ti 2*p* core line of $SrTiO_3$, measured with the same energy resolution. For the 5-u.c. conducting sample, the full width at half maximum (FWHM) of the Ti $2p_{3/2}$ peak (1.47 eV) is larger than that of the 5-u.c. (1.41 eV) and the 3-u.c. (1.43 eV) insulating samples. It is important to note that the narrower Ti 2*p* peak is that of STO (1.36 eV). Therefore, we see an overall decrease of the Ti 2*p* FWHM from the conducting LAO-STO to the insulating STO single crystal. We exclude broadening effects due to charging, which should be opposite to those observed, and therefore we regard the broadening as due to an intrinsic effect. Also the peak area of Ti^{3+} states of the conducting compound is larger than that of the two insulating compounds. The Ti^{3+}/Ti^{4+} ratio sharply decreases from 0.056 (5 u.c.) to 0.012 (3 u.c.) and is nearly negligible for the 5-u.c. insulating sample (0.006) and the STO single crystal (0.004), assuming an uncertainty of ± 0.005 on the peak ratio values. Furthermore, the Ti^{3+} BE of the samples grown in low P_{O_2} is different from that measured for the other samples, the insulating 5 u.c. and the reference STO single crystal. This peak is found about 2 eV below the main line, but this difference is reduced when the 5-u.c. insulating (1.78 eV) and the STO (1.73 eV) samples are considered, indicating a different origin for these peaks. Indeed, an insulating sample has been reported[18] to show a Ti^{3+} peak closer to the main line with respect to a conducting LAO-STO interface.

The presence of Ti^{3+} states was controversial in early studies on LAO-STO, as not all authors observed these features in spite of the conducting nature of their samples. As already mentioned, a signature of Ti^{3+} states is the feature appearing on the low-BE side of the Ti $2p_{3/2}$ core line. In addition, this feature should have a counterpart in the valence-band region, detectable either through RESPES at the Ti *L* edge or through ultraviolet photoemission spectroscopy (UPS).[30] While Takizawa *et al.*[19] and Yoshimatsu *et al.*[28] discuss the properties of Ti 2*p* core lines, in Segal *et al.*'s study[21] no

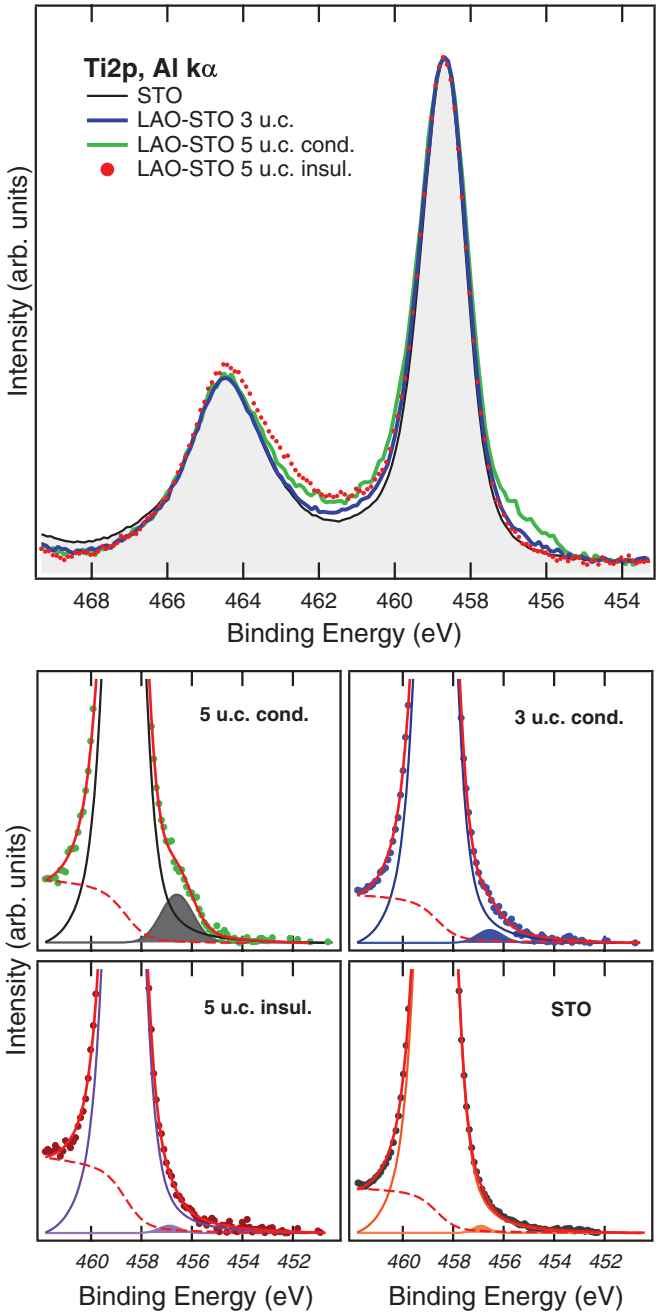

FIG. 4. (Color online) (top) Ti $2p$ core-level XPS spectra collected from the 3-u.c insulating HS (thick line), the 5-u.c. conducting HS (thin line), the 5-u.c. insulating HS (dots), and the STO single crystal (shaded area). (bottom) Fitting (thin lines) of the Ti $2p_{3/2}$ core levels (dots) with two peaks, accounting for the Ti^{4+} and the Ti^{3+} (shaded area) contributions, and an integral (Shirley type, dashed line) background.

mention is made of Ti $2p$. Yoshimatsu *et al.* do not report on the Ti^{3+} contribution, but they focus on the BE shift of the Ti $2p_{3/2}$ core line, while Takizawa *et al.* discuss the Ti^{4+}/Ti^{3+} ratio but do not report on the Ti $2p_{3/2}$ BE shift. Furthermore, unlike more recent studies,[17,18] Yoshimatsu *et al.*[28] do not find any evidence of $3d^1$ states in RESPES experiments at the Ti L-edge resonance. For the present samples, evidence of Ti $3d$ states in the gap are provided in Ref. 29 (Chap. 5).

In addition to Ti $2p$, the Sr $3d$ core levels of the heterostructures appear to be different from those of STO [Fig. 1(c)]. As shown in Table II, in spite of the high quality of the STO side of the heterojunction, the Sr peaks are not as sharp as pristine STO. The Sr $3d$ peak of the conducting 5-u.c. sample (1.24 eV) is larger than that of the corresponding 3-u.c. layer (1.18 eV), with both being larger than the peak measured for STO (1.05 eV). The results of the Sr $3d$ core-level fitting with Gaussian line shapes are shown in the bottom panel of Fig. 1. This trend is consistent with that measured for the Ti $2p$ core lines, suggesting the presence of disorder (cationic exchange or oxygen vacancies) around strontium atoms at the interface. This structural disorder is supposed to alter the ideal structural environment around the Ti and Sr cations, yielding potential fluctuations that ultimately may result in a Ti $2p$ and Sr $3d$ peak width broadening. Similar effects have been observed in, e.g., the Ti $2p$ core lines of Fe-doped rutile single crystals.[31]

An alternative picture to be considered that is, however, supported by a qualitative analysis is based on possible band-bending effects on the peak width. Segal *et al.*[21] have considered this hypothesis, and they have been able to estimate a band bending smaller than that expected from theoretical predictions. Indeed, Segal *et al.*[21] have investigated these effects on the La $4d_{3/2}$ peak width, obtaining quite smaller broadening with respect to those expected from the polar catastrophe theory. Furthermore they do not find a specific trend in the FWHM, as the data appear to be scattered.

In the present study we choose to address this question on the elements (Sr and Ti) of the buried interface. Assuming that the increase of peak width is due to band bending, it is interesting to relate the observed FWHM to the VBO by comparing the results of Tables I and II. Here, the Ti $2p$ peak width in STO (1.36 eV) is regarded as the width of the "ideal" Ti-terminated STO without the LAO capping layer. Based on this, we can extract the extra width σ_{EXTRA} due to the interface effects on the basis of the following equation: $\sigma_{\mathrm{TOTAL}} = (\sigma^2_{\mathrm{STO}} + \sigma^2_{\mathrm{EXTRA}})^{1/2}$. The results are reported in Table I. As can be observed, σ_{EXTRA} shows a decrease similar to that found for the average core-level shift that appears in Table II. This indicates that larger average core-level shifts yield larger Ti $2p$ peak widths.

Finally, from the Ti^{3+}/Ti^{4+} intensity ratio, by properly considering the attenuation of the Ti signal due to the LAO overlayer, an estimation of the sheet charge density (SCD) can also be provided. The evaluation of the Ti^{3+}/Ti^{4+} ratio has been drawn on the basis of the DDF concept, using the XPS peak area values reported in Table I. The results are shown in Fig. 5. Our calculations are based on the fact that the Ti^{3+}/Ti^{4+} ratio reported in Table I can be generated by different distributions of the Ti^{3+} ions below the interface; for example, the same ratio can be produced by a high density of ions close to the interface or by a low density of ions distributed across a larger layer below the interface. We start our analysis by assuming that, once the width of the charge profile is established, the Ti^{3+} ion distribution is constant below the interface. A different profile, e.g., a charge profile decaying with depth below the interface, can be ultimately described by a linear combination of constant charge profiles, as our

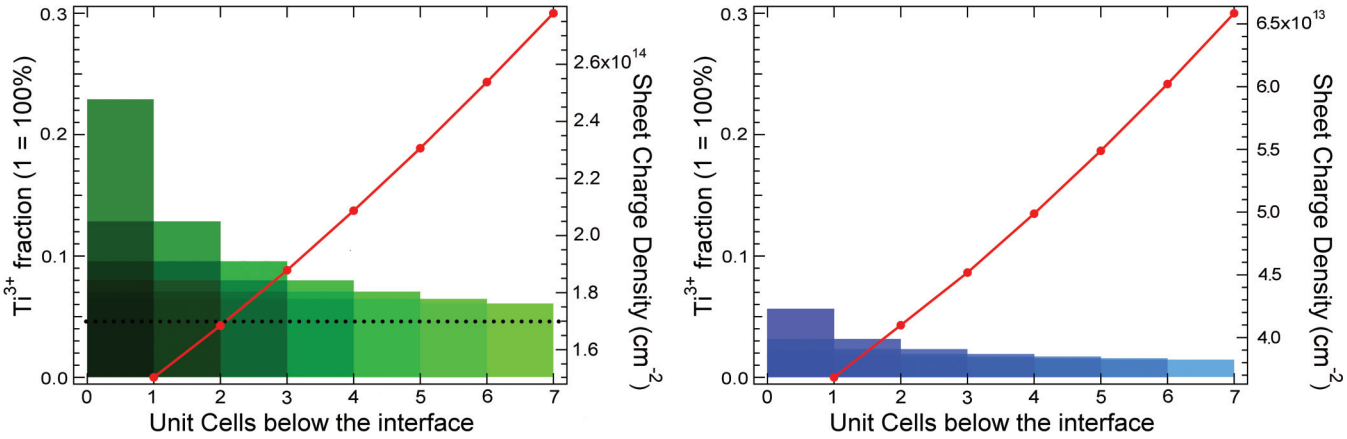

FIG. 5. (Color online) Charge profile and corresponding sheet charge density for (left) the 5-u.c. sample and (right) the 3-u.c. sample.

calculation is carried out on quite fine discrete steps (i.e., the thickness of a unit cell).

In Fig. 5 the height of the histogram bars represents the Ti^{3+} fraction predicted for a uniform distribution of Ti^{3+} atoms in a layer below the interface as thick as the width of the histogram bar. The thickness of this layer is assumed to be a multiple of the STO unit cell parameter. The corresponding SCD is evaluated for each histogram bar and is shown as a thick line (right axis). Assuming that all the Ti^{3+} ions are located in the first unit cell below the interface, the resulting SCD is 1.5×10^{14} cm^{-2}. This value represents the lowest limit for the SCD calculated on the basis of the experimental Ti^{4+}/Ti^{3+} XPS peak area ratio.

A much lower estimation of the sheet charge density is drawn for the insulating 3-u.c. sample. In this case, the lowest limit for the SCD is 3.7×10^{13} cm^{-2}. This value can be regarded as the intrinsic density of carriers at the interface for the two samples grown at low P_{O_2}, which is found independently of the physical mechanisms underlying the 2DEG buildup.

The estimated SCD value for the 5-u.c. conducting sample can be compared to transport measurements carried out on a 5-u.c sample grown under the same conditions. The data are shown in Fig. 6, where the carrier density and the mobility dependence on temperature are reported in the top and bottom panels, respectively. As can be observed, the carrier density increases with temperature, reaching a *plateau* above $T = 200$ K, with a carrier density of 1.7×10^{14} cm^{-2}. This experimental value is also shown in Fig. 5 as a dashed horizontal line. The matching between the transport measurements data and the SCD estimation based on XPS data occurs provided that the estimated SCD curve (solid line in Fig. 5) lies above the measured carrier density (dashed line in Fig. 5), i.e., by assuming that the SCD is spread at least 2 u.c. below the interface. Therefore, the combination of transport and XPS data analysis provides here a lower limit for the extent of the SCD below the interface.

If we consider a constant charge density spread about 2 u.c. below the interface, the present results are in good agreement with those reported by Sing *et al.* on the basis of HAXPES experiments.[20]

As noted above, the SCD resulted to be nonzero also for the 3-u.c. sample (3.7×10^{13} cm^{-2}). This seems to point out that only a fraction (about 75%) of the Ti^{3+} states detected by XPS can contribute to the 2DEG. One explanation can be found in Ref. 32, where a distinction between two kinds

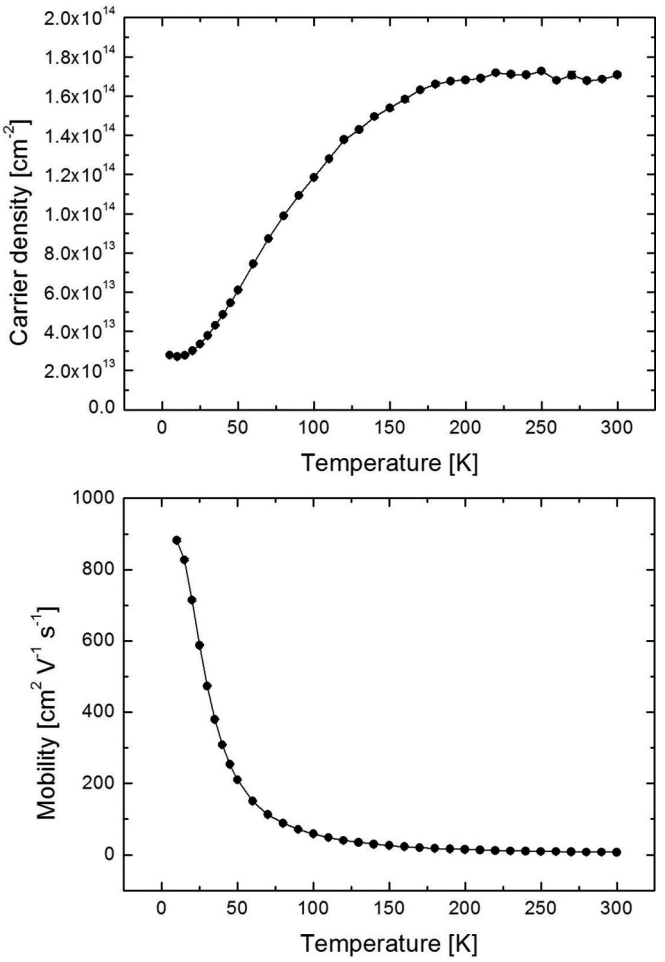

FIG. 6. Transport measurements on a 5-u.c. conducting sample. (top) Carrier density and (bottom) mobility.

of charge carriers is provided: low-density, high-mobility carriers for the transport measurements and high-density, low-mobility carriers from optical measurements. Alternatively, the formation of photoinduced charge carriers either by x-ray or ambient light irradiation has to be considered. However, under this assumption, it is not straightforward to explain the lack of such large photoinduced effects in the insulating 3-u.c. sample and also in STO. In particular, as these effects should occur on the STO side of the junction to yield Ti^{3+} electronic states, it is difficult to justify the lower density for the 3-u.c. sample, where irradiation effects are supposed to be larger than in the 5-u.c. sample due to the thinner LAO overlayer on top of the STO substrate.

Finally, we observe that an estimate of the Ti^{3+} fraction carried out with the IMFP attenuation length alone, without considering the full DDF approach, would overestimate the Ti^{3+} fraction because, neglecting, e.g., the elastic scattering events, the resulting attenuation length is higher. Namely, by using the IMFP for STO ($\lambda = 21.67$ Å at $E_k = 1000$ eV) we would obtain a Ti^{3+} fraction of 0.34 rather than 0.23 for a distribution depth of 1 u.c. and 0.19 rather than 0.12 for a distribution depth of 2 u.c., i.e., an overall overestimation of about 50% . This would yield an analogous overestimation of the SDC.

IV. CONCLUSIONS

Far from being thoroughly assessed in the literature, the spectroscopic signature of 2DEG in LAO-STO interfaces is discussed in the present study, where we add data to the set of experiments so far reported. Indeed, rather than focusing on the difference between p-type and n-type samples, we choose to focus on oxygen stoichiometry effects and on the comparison with parent LAO and STO compounds. Unlike previous studies, we show that in LAO-STO heterostructures (i) the Ti^{3+} contribution to Ti $2p$ core levels, (ii) the Ti $3d^1$ in-gap states,[29] and (iii) a larger Ti $2p$ width with respect to STO can be simultaneously present, although at different extents, suggesting that all these signatures of the 2DEG are accessible via photoemission on each sample.

Three LAO-STO interfaces have been analyzed by x-ray photoemission spectroscopies, along with LAO and STO reference single crystals. The energy, width, and intensity of core-level peaks and the valence band spectra have been carefully considered in order to look for band-bending effects at the heterointerface and to probe the dependence of the Ti^{3+} charge density on the growth conditions.

In the analysis of VBO, we consider the approach suggested by Chambers *et al.*[8] by referencing the BE also to separated LAO and STO valence-band maxima. Unlike the reported findings, we find BE differences sensitive to the choice of elements, which suggests that different atoms in the interface may undergo different energy shifts. In particular, when Ti is involved, the major differences are estimated.

From the analysis of core-level energies, we exclude the presence of band-bending effects larger than about 0.7 eV, ruling out tunneling from the LAO offset valence band to STO empty $3d$ levels as the sole mechanism for the buildup of the 2DEG. Differences in band offset among the three samples are quite limited, spanning a range of about 0.2 eV, in spite of the remarkably different growth conditions and electrical properties. Likewise, differences among relative BE shifts required to best fit the LAO-STO valence band are small. However, a correlation among these differences, the peak widths of Ti and Sr at the interface, and band bending is found, showing that band offset is at work to shape the energy landscape and that it is possible to consistently single out these effects by a careful analysis of spectroscopic data. Indeed, the FWHM of the Ti $2p$ and Sr $3d$ core lines is larger for the conducting sample with respect to any of the insulating interfaces and the STO single crystal. The intrinsic origin of this width is ascribed to band-bending effects, although disorder effects (electronic or structural) around the photoemitting atom in the conducting sample may be at work at the same time.

Finally, we have shown that the density of Ti^{3+} levels strongly depends both on the LAO overlayer thickness and oxygen partial pressure during the growth. Two heterostructures grown at the same P_{O_2} present a well-detectable Ti^{3+} peak about 2 eV below the Ti^{4+} main line. The STO and the 5-u.c. insulating samples show a much weaker contribution of Ti^{3+} states, with also a different binding energy.

On the basis of the Ti^{3+}/Ti^{4+} XPS peak area ratio, SCD of the 5-u.c. layer turns out to be about four times larger than in the 3-u.c. sample. Direct comparison with transport measurements on the 5-u.c. conducting sample allowed us to set a lower limit for the extent of the 2DEG below the interface.

ACKNOWLEDGMENTS

Support from the Dutch FOM and NWO foundations is acknowledged.

[1] H. Y. Hwang and A. Ohtomo, Nature (London) **427**, 423 (2004).
[2] S. Thiel, G. Hammer, A. Schmehl, C. W. Schneider, and J. Mannhart, Science **313**, 1942 (2006).
[3] R. Pentcheva and W. E. Pickett, J. Phys. Condens. Matter **22**, 043001 (2010).
[4] N. Nakagawa, H. Y. Hwang, and D. A. Muller, Nat. Mater. **5**, 204 (2006).
[5] J. Gonjakowski, F. Finocchi, and C. Noguera, Rep. Prog. Phys. **71**, 016501 (2008).
[6] N. Reyren, S. Thiel, A. D. Caviglia, L. Fitting Kourkoutis, G. Hammerl, C. Richter, C. W. Schneider, T. Kopp, A. S. Rüetschi, D. Jaccard, M. Gabay, D. A. Muller, J. M. Triscone, and J. Mannhart, Science **317**, 1196 (2007).
[7] A. Brinkman, M. Huijben, M. van Zalk, J. Huijben, U. Zeitler, J. K. Maan, W. G. van der Wiel, G. Rijnders, D. H. A. Blank, and H. Hilgenkamp, Nat. Mater. **6**, 493 (2007).
[8] S. A. Chambers, M. H. Englehard, V. Shutthanandan, Z. Zhu, T. C. Droubay, T. Feng, H. D. Lee, T. Gustafsson, E. Garfunkel, A. Shah, J. M. Zuo, and Q. M. Ramasse, Surf. Sci. Rep. **65**, 317 (2010).

[9]V. Vonk, J. Huijben, D. Kukuruznyak, A. Stierle, H. Hilgenkamp, A. Brinkman, and S. Harkema, Phys. Rev. B **85**, 045401 (2012).
[10]R. Yamamoto, C. Bell, Y. Hikita, H. Y. Hwang, H. Nakamura, T. Kimura, and Y. Wakabayashi, Phys. Rev. Lett. **107**, 036104 (2011).
[11]R. Pentcheva and W. E. Pickett, Phys. Rev. Lett. **102**, 107602 (2009).
[12]A. S. Kalabukhov *et al*., Phys. Rev. Lett. **103**, 146101 (2009).
[13]G. Herranz *et al*., Phys. Rev. Lett. **98**, 216803 (2007).
[14]W. Siemons, G. Koster, H. Yamamoto, W. A. Harrison, G. Lucovsky, T. H. Geballe, D. H. A. Blank, and M. R. Beasley, Phys. Rev. Lett. **98**, 196802 (2007).
[15]M. Basletic, J.-L. Maurice, C. Carrétéro, G. Herranz, O. Copie, M. Bibes, É. Jacquet, K. Bouzehouane, S. Fusil, A. Barthélémy, Nat. Mater. **7**, 621 (2008).
[16]G. Rijnders and D. H. A. Blank, Nat. Mater. **7**, 270 (2008).
[17]G. Drera, F. Banfi, F. Federici Canova, P. Borghetti, L. Sangaletti, F. Bondino, E. Magnano, J. Huijben, M. Huijben, G. Rijnders, D. H. A. Blank, H. Hilgenkamp, and A. Brinkman, Appl. Phys. Lett. **98**, 1 (2011).
[18]A. Koitzsch, J. Ocker, M. Knupfer, M. C. Dekker, K. Dörr, B. Buchner, and P. Hoffmann, Phys. Rev. B **84**, 245121 (2011).
[19]M. Takizawa, S. Tsuda, T. Susaki, H. Y. Hwang, and A. Fujimori, Phys. Rev. B **84**, 245124 (2011).
[20]M. Sing, G. Berner, K. Goss, A. Muller, A. Ruff, A. Wetscherek, S. Thiel, J. Mannhart, S. A. Pauli, C. W. Schneider, P. R. Willmott, M. Gorgoi, F. Schafers, and R. Claessen, Phys. Rev. Lett. **102**, 176805 (2009).
[21]Y. Segal, J. H. Ngai, J. W. Reiner, F. J. Walker, and C. H. Ahn, Phys. Rev. B **80**, 241107 (2009).
[22]J. J. Yeh and I. Lindau, At. Data Nucl. Data Tables **32**, 1 (1985).
[23]I. S. Tilinin, A. Jablonski, J. Zemek, and S. Hucek, J. Electron Spectrosc. Relat. Phenom. **97**, 127 (1997).
[24]W. S. M. Werner, Surf. Int. Anal. **31**, 141 (2001).
[25]A. Jablonski, Phys. Rev. B **58**, 16470 (1998).
[26]L. Qiao, T. C. Droubay, T. Varga, M. E. Bowden, V. Shutthanandan, Z. Zhu, T. C. Kaspar, and S. A. Chambers, Phys. Rev. B **83**, 085408 (2011).
[27]M. F. Sunding, K. Hadidi, S. Diplas, O. M. Løvvik, T. E. Norby, A. E. Gunnæs, J. Electron Spectrosc. Relat. Phenom. **184**, 399 (2011).
[28]K. Yoshimatsu, R. Yasuhara, H. Kumigashira, and M. Oshima, Phys. Rev. Lett. **101**, 026802 (2008).
[29]G. Drera, arXiv:1210.8000.
[30]W. Siemons, G. Koster, H. Yamamoto, T. H. Geballe, D. H. A. Blank, and M. R. Beasley, Phys. Rev. B **76**, 155111 (2007).
[31]L. Sangaletti, M. C. Mozzati, G. Drera, P. Galinetto, C. B. Azzoni, A. Speghini, and M. Bettinelli, Phys. Rev. B **78**, 075210 (2008).
[32]S. S. A. Seo, Z. Marton, W. S. Choi, G. W. J. Hassink, D. H. A. Blank, H. Y. Hwang, T. W. Noh, T. Egami, and H. N. Lee, Appl. Phys. Lett. **95**, 082107 (2009).